




# Femtosecond pulse laser-engineered glass flexible structures instrumented with an in-built Bragg grating sensor

MATEO TUNON DE LARA,<sup>1,2</sup> LOÏC AMEZ-DROZ,<sup>2,3</sup>  
KARIMA CHAH,<sup>1</sup>  PIERRE LAMBERT,<sup>2</sup> CHRISTOPHE COLLETTE,<sup>3,4</sup>  
AND CHRISTOPHE CAUCHETEUR<sup>1,\*</sup> 

<sup>1</sup>Electromagnetism and Telecommunication Department, UMONS, Mons, Belgium

<sup>2</sup>TIPs Department, CP 165/67, Université Libre de Bruxelles, 50 av FD Roosevelt, B- 1050 Brussels, Belgium

<sup>3</sup>Department of Aerospace and Mechanical Engineering, Université de Liège, Liège, Belgium

<sup>4</sup>BEAMS Department, CP 165/56, Université Libre de Bruxelles, 50 av FD Roosevelt, B- 1050 Brussels, Belgium

\*christophe.caucheteur@umons.ac.be

**Abstract:** The advent of near-infrared femtosecond pulse laser has enabled the highly-resolved manufacturing of micro/nano structures in various materials including glass. In this paper, we make use of an automated femtosecond laser system, so-called Femtoprint, to design a monolithic self-instrumented mechanism that we use for in-built strain sensing. To that aim, a flexible structure is designed and produced from a silica planar substrate. It has a flexural joint in which an optical waveguide and a Bragg grating have been directly inscribed using femtosecond pulse laser. The latter provides a non-destructive and non-intrusive measurement tool. The axial strain sensitivity of the in-built Bragg grating has been experimentally determined to be 1.22 pm/ $\mu\epsilon$ , while its temperature sensitivity is 10.51 pm/ $^{\circ}\text{C}$ . The demonstration of such instrumented glass flexible mechanisms paves the way towards a new class of highly integrated sensors suitable for applications at the microscale or in harsh environments.

© 2023 Optica Publishing Group under the terms of the [Optica Open Access Publishing Agreement](#)

## 1. Introduction

Femtosecond pulse lasers are powerful tools used in a variety of industrial applications [1]. A prominent example remains the processing of glass using femtosecond pulse laser [2]. This process involves the use of a tightly-focused high-powered laser beam to create precise cuts, holes, and patterns within the glass and on its surface. The laser beam can be focused to a very small spot size, such as the non-linear modification can happen in a confined volume that can be smaller than the focal volume. This level of precision is not possible with traditional mechanical or chemical methods. Moreover, the short pulses allow for precise control of the amount of energy delivered to the glass, minimizing heat damage and ensuring high-quality cuts. Depending on the desired outcome, the focused laser beam is usually moved across the glass structure in a predetermined pattern, or focused at specific points to create holes or channels. The process can be controlled using computer software to ensure precise and repeatable results. Complex 3D structures can also therefore be generated by using multiple laser beams focused at different depths [3]. This technique is known as femtosecond laser-assisted chemical etching and has a wide range of potential applications, such as creating microfluidic channels or optical components [4]. The mechanism of the material modification under focused femtosecond pulse laser has been the subject of intense research [4–6]. In glass, it has been demonstrated that three types of material modification can be generated depending on the properties of the used femtosecond pulse laser [5,7–9], i.e. pulse energy and duration [5,7], repetition rate and scanning

speed and scanning speed and direction as well as polarization [10]. Hence, with increasing energy density levels the silica glass undergoes different structural changes:

- Densification [11,12], which induces a local and isotropic modification of the refractive index at the focal point and can lead to the creation of optical waveguides [13,14].
- Nano-grating corresponding to a structural change of the material that usually takes the form of an alternation of fused silica nanoplanes and nanochannels perpendicular to the incident polarization of the laser beam [7].
- Direct ablation is the scenario where the energy of the pulse is amplified to a significant degree, resulting in void creation within the exposed material sample [3,15].

The same laser pulse energy as for the creation of nano-gratings can also be used for the creation of mechanical structures. Indeed, the glass material that has undergone laser modification is more sensitive to chemical attack than unmodified areas. An etching rate difference between the two areas of about two orders of magnitude provides etching selectivity. Accordingly, the laser pulses pattern the material to create a structure to be etched (removed chemically) leaving out the unmodified parts. The etching process can be conducted in different types of solutions. It can either be KOH [16,17], HF [18] or NaOH [19].

The main elements of our advanced sensing platforms are Bragg gratings. The latter is much more known in optical fibres than in planar waveguides. In the following, we briefly recall how they can be used for sensing purposes. Fig. 1(a) represents the inscription of a grating in an optical fibre using femtosecond pulse laser while Fig. 1(b) depicts the standard geometry of a telecommunication-grade single-mode optical fibre and displays its interaction with a Bragg grating. A picture of a Bragg grating manufactured in the fibre core was taken with the microscope (Fig. 1(c)). Fig. 1(d) and Fig. 1(e) show how the characterisation of a fibre Bragg grating according to temperature occurs. The simulation of the reflected spectrum was realised with the Matlab software. To do so we decided to follow the theoretical equation of Ugale [20]. We conducted a simulation of a Bragg grating, setting the refractive index to  $n_{\text{eff}} = 1.45$ . The maximum permissible change in refractive index was  $\delta_n = 0.0001$ . The Bragg grating exhibited a refractive index modulation period of  $\Lambda = 530$  nm. Several measurements are taken at different temperatures and then a linear curve is plotted to observe the evolution of the Bragg wavelength as a function of temperature.

Bragg gratings are sensitive to temperature and axial strain. The axial strain is defined as  $\epsilon = \frac{\Delta\Lambda}{\Lambda}$  with  $\Lambda$ , the refractive index modulation period. It can be obtained from the Bragg wavelength shift  $\Delta\lambda_{\text{BG}}$ . This shift is coupled with the temperature effect  $\frac{\Delta\lambda_{\text{BG}}}{\Delta T}$  and the mechanical strain effect  $\frac{\Delta\lambda_{\text{BG}}}{\Delta\epsilon}$ . The complete development can be found in [21].

$$\Delta\lambda_{\text{BG}} = 2 \left( \Lambda \frac{dn_{\text{eff}}}{dT} + n_{\text{eff}} \frac{d\Lambda}{dT} \right) \Delta T + 2 \left( \Lambda \frac{dn_{\text{eff}}}{d\epsilon} + n_{\text{eff}} \frac{d\Lambda}{d\epsilon} \right) \Delta\epsilon \quad (1)$$

The term in Eq. (1) relying on the temperature can be described as :

$$\frac{\Delta\lambda_{\text{BG}}}{\Delta T} = \lambda_{\text{BG}} \left( \frac{1}{n_{\text{eff}}} \frac{dn_{\text{eff}}}{dT} + \frac{1}{\Lambda} \frac{d\Lambda}{dT} \right) \quad (2)$$

$\frac{1}{n_{\text{eff}}} \frac{dn_{\text{eff}}}{dT}$  is the thermo optic-coefficient, whereas  $\frac{1}{\Lambda} \frac{d\Lambda}{dT}$  is the thermal expansion coefficient. In the case of a germanium-doped silica core optical fibre, the thermo-optic coefficient is about  $8.6 \cdot 10^{-6} \text{K}^{-1}$ . Concerning the thermal coefficient, it is about  $0.55 \cdot 10^{-6} \text{K}^{-1}$  for silica. With the defined  $\lambda_{\text{BG}} \approx 1589$  nm, it gives a theoretical sensitivity to the temperature of  $10 \text{ pm}/^\circ\text{C}$ . Using

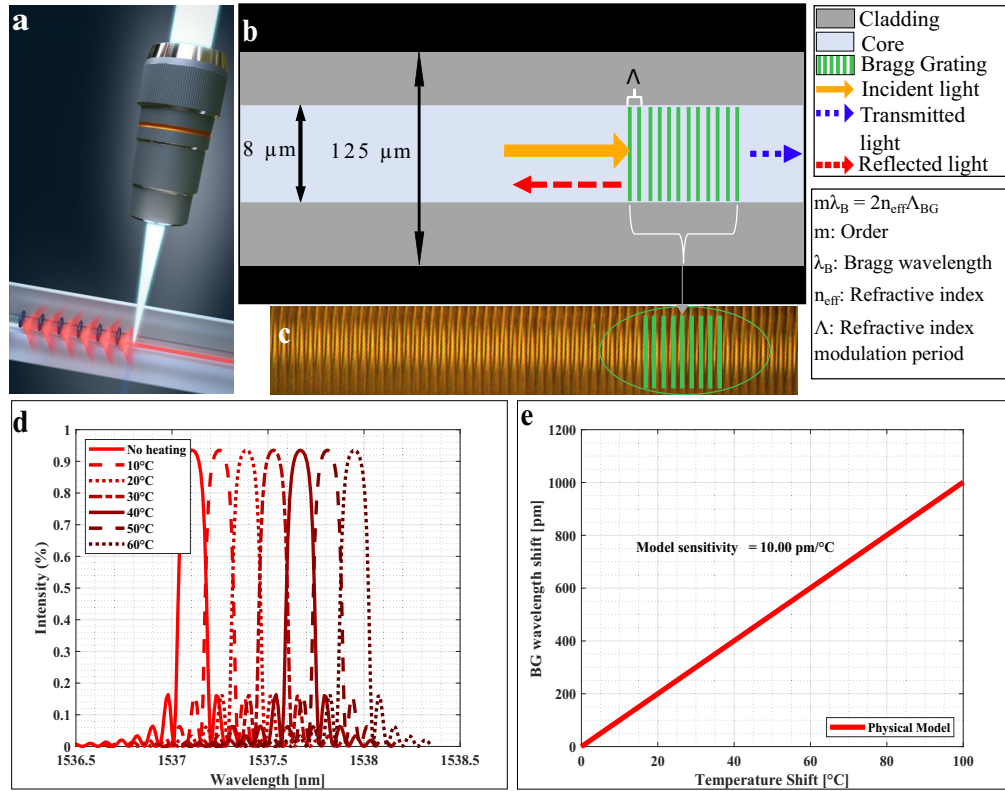


**Fig. 1.** **a** Artistic view of the creation of controlled defects in optical fibres using focused femtosecond pulse laser. **b** Schematic representation of a Bragg grating in the fibre core. **c** Optical microscope picture of a Bragg grating in an optical fibre inscribed with a femtosecond laser. **d** Simulation of the effect of the temperature on the reflected amplitude spectrum of a Bragg grating. **e** Bragg wavelength shift as a function of temperature. The characterisation in **e** can also be conducted with a traction applied to the Bragg grating.

the definition of the Bragg wavelength the strain-dependent term in Eq. (1) can be rewritten as:

$$\frac{\Delta\lambda_{\text{BG}}}{\Delta\epsilon} = \lambda_{\text{BG}}(1 - p_e) \quad (3)$$

For silica glass, which is an isotropic material, the strain-optic constant  $p_e$  can be obtained from [21] as :

$$p_e = \frac{n_{\text{eff}}^2}{2} [p_{12} - \nu(p_{11} + p_{12})] \quad (4)$$

with  $p_{11}$  and  $p_{12}$ , the elasto-optic independent coefficients for bulk silica ( $p_{11} = 0.121$  and  $p_{12} = 0.270$ ), listed in [22],  $\nu$  and  $n_{\text{eff}}$ , respectively its Poisson's ratio and the effective refractive index ( $\nu = 0.16$  and  $n_{\text{eff}} = 1.45$ ). With the defined  $\lambda_{\text{BG}} \approx 1589$  nm, it gives a theoretical sensitivity to an axial strain of 1.24 pm/ $\mu\epsilon$ .

For the grating inscription, unlike the standard writing methods with ultra-violet continuous or nanosecond pulse laser, the advent of tight focusing of femtosecond pulse laser has allowed, through nonlinear absorption and tight focusing, to produce gratings in different materials including pure silica [23]. Typically, each pulse of the femtosecond laser engraves permanently one period of the grating through a nonlinear absorption process. In optical fibres, Bragg

gratings are usually produced by the point-by-point [24], line-by-line [11] or plane-by-plane [25] manufacturing processes and show unprecedented resistance among the photonic sensing devices to high temperature and harsh environment [26]. Temperature sensing up to 1050 °C has been successfully reported [27]. Driven by the need and advances in technology, numerous companies developed femtosecond pulse laser-induced FBGs nowadays. Besides, the planar glass substrates processing by femtosecond laser has attracted the attention of researchers thanks to the many possibilities they offer for device integration [1,2]. Efforts have been made to optimize pulse laser parameters [7,8], beam shaping [28], waveguide design [29], to produce low-loss waveguides [30], waveguide and Bragg grating within, [26,31] and many other optical components.

Hence, vibration monitoring with monolithic glass sensors produced by etching-assisted femtosecond laser machining technology has been reported [32,33]. Athanasiou and his team used the beam as a tool to test the material at the microscale. The same femtosecond laser was used to produce and test the device. This method is destructive, however, it provides insight into the material properties at the microscale. In [32], Casamenti and his team optically exploit the mechanical non-linearities intrinsically present in the suspended double-clamped beam to determine the stress build-up due to vibration. The principle is to measure the vibration induced-phase modulation of the coherent light travelling through the beam. This device uses an integrated Mach-Zehnder interferometer combining one reference arm with the arm through the suspended beam. This interferometric technique is precise and robust. Nevertheless, it requires transmission measurement. In our work, we have designed and developed an instrumented glass flexible structure featuring an in-built Bragg grating sensor in its flexible part, entirely manufactured using a fully-automated femtosecond pulse laser process. Silica was chosen as raw material for this sensing platform due to its flexible properties. It has an elastic range ratio of about 0.02 (its bending strength over Young's modulus). For comparison with other compliant mechanism materials, the elastic range ratio of steel and TiAl6V4 are respectively 0.004 and 0.007. Therefore, fused silica is a suitable candidate for a force-sensitive element. It has also a low thermal expansion ( $5.3 \times 10^{-7}/^{\circ}\text{C}$ ), a key factor for precision mechanics. It has a high elastic limit ( $>1$  GPa) to the Young modulus (72 GPa) ratio, very useful for elastic deformation in large-range and high-resolution force sensors. Its low internal damping is suitable for resonant sensors and long-term stability. This set of properties can be used to overcome the different limitations of other sensor technologies. The high temperature of glass transition ( $T_g = 1480$  K) of silica and its low thermal expansion allows to reach a temperature above 800 °C [34,35] without any major deformation, while femtosecond pulse laser-induced gratings can survive these high temperatures [27]. For all these reasons, silica is a very appealing material for the production of highly-integrated flexible structures. However, the controlled design of flexible instrumented glass structures at the micro-scale remains challenging as it requires to master the femtosecond pulse laser micro-machining process. To that aim, we use an automated system, the Femtoprint process [36], to tightly shape and instrument a flexible structure starting from a standard glass planar substrate. The core element of our integrated sensing platform is a Bragg grating within a waveguide inscribed in a flexible structure produced from a monolithic fused silica glass. To achieve this in-built sensing mechanism, a dedicated optical waveguide and a specific holder for a connecting optical fibre were designed and manufactured beforehand using the femtosecond pulse laser process. For each part of the process (shaping of the flexible structure, creation of the waveguide, inscription of the Bragg grating and creation of the mechanical holder), the femtosecond pulse laser has been optimized in terms of pulse energy, polarization, repetition rate, displacement speed and path. It is noteworthy that while fibre Bragg gratings typically measure traction/compression strain, the bending structures that we have developed allow for significantly larger strains under the same external force. This improvement in strain magnitude leads to an enhanced resolution in force measurement (we expect to compete with the state of the art of FBG instrumented medical instruments with a standard analyzer with 1 pm

resolution: 1, 2, 3 orders of magnitude more resolute analyzers will consequently allow 1, 2, 3 orders of magnitude more resolute force measurement). This platform can be used in numerous applications. The primary focus of our work is the maximum elastic strain exhibited by the system. The integration of the sensors plays a crucial role as a fundamental prerequisite, enabling the subsequent creation of intricate and distinct structures within the confines of a single glass plate [37]. The fully-developed platform was calibrated for axial strain sensing and its response to temperature was also investigated. Experimental strain and temperature sensitivity values were determined to be 1.22 pm/ $\mu\epsilon$  and 10.51 pm/ $^{\circ}\text{C}$ , respectively. They are in line with the theoretical predictions. The exact design of the flexible structure results from mechanical considerations that will be summarized hereafter. Hence, compared to the state-of-the-art solutions, the main originalities of our work arise from the production of instrumented glass flexible structures encompassing an optimized holder for the connecting optical fibre. The successful demonstration of such instrumented glass flexible mechanisms brings a new class of highly integrated sensors that can be optimized for a large range of applications, also in more stringent environments, e.g. when the sensors are surrounded by liquid or subject to high-temperature gradients.

## 2. Methods

### 2.1. Fabrication

In our work, the material is a planar substrate of silica glass (25 mm large, 70 mm long). The deposited energy per surface unit, or net fluence, quantifies the femtosecond laser impact on the silica glass, both at its surface and in depth [38]. This parameter is an approximation of how many joules per square metres are localised on the material:

$$\Phi_d = \frac{4e_p}{\pi\omega_n} \left(\frac{f}{v}\right) \quad (5)$$

The deposited energy per unit surface ( $\Phi_d$ ) depends on several parameters. The energy of the pulse ( $e_p$ ), the writing speed ( $v$ ), the repetition rate ( $f$ ) and the non-linear beam waist. The latter cannot be adjusted, as it is linked to the microscope objective used to focus the laser beam (In the current case, the objective is a LMH-20x-1064 from Thorlabs). Depending on its value, the pulse energy will induce different kinds of modifications on the material (cf. Introduction). In the femtosecond laser-assisted etching process (Fig. 2(a)–2(c)), the same laser is used to manufacture both optical and mechanical structures. Optical structures (waveguides and gratings in our case) are entirely produced with femtosecond pulse laser. Mechanical structures (shaping) require an additional wet etching process to remove parts of materials that have been previously exposed to laser pulses. Hence, different laser pulse energies are selected to perform these respective tasks. They result from an optimization process that was conducted in the early stage of our work. It turns out that a pulse energy of 130 nJ (The pulse duration is  $< 300$  fs, the wavelength of the femtosecond laser is 1030 nm, the Numerical Aperture of the objective is 0.4) is suited to obtain a densification of the silica glass and thus an increase of the refractive index. This is therefore the value chosen for the creation of waveguides and Bragg gratings. The trajectory and velocity are adjusted according to the intended modification. In the case of mechanical shaping, the pulse energy reaches 230 nJ while the repetition rate is set to 1 MHz and the writing speed is 950 mm/min. For optical inscription, the energy output of the energy of the pulse is limited to 130 nJ, but the repetition rate remains 1 MHz and the inscription speed is decreased to 20 mm/min. It is also important to know that due to the presumed size of the voxel and because we wanted to have a waveguide and a Bragg grating in the middle of the plate, an adjustment was made. The voxel is supposed to be 20  $\mu\text{m}$  thick so the inscription of the waveguide and the Bragg grating starts at 240  $\mu\text{m}$  from the surface. All the parameters of inscription are summarized in Table 1. In all cases, the laser path used for the patterning is numerically controlled. To precisely define this

**Table 1.** Table summarizing different parameters of inscription in function of the intended modification

Type of modification	Energy pulse	Repetition rate	Translation speed
Waveguide	130 nJ	1000 kHz	20 mm/min
Bragg Grating	150 nJ	1000 kHz	15 mm/min
Mechanical structures	230 nJ	1000 kHz	950 mm/min

path, a solid model of the monolithic structure is first designed using the SolidWorks software. Then, the shape of the solid is exported to the custom Alphacam software version provided by FEMTOprint.

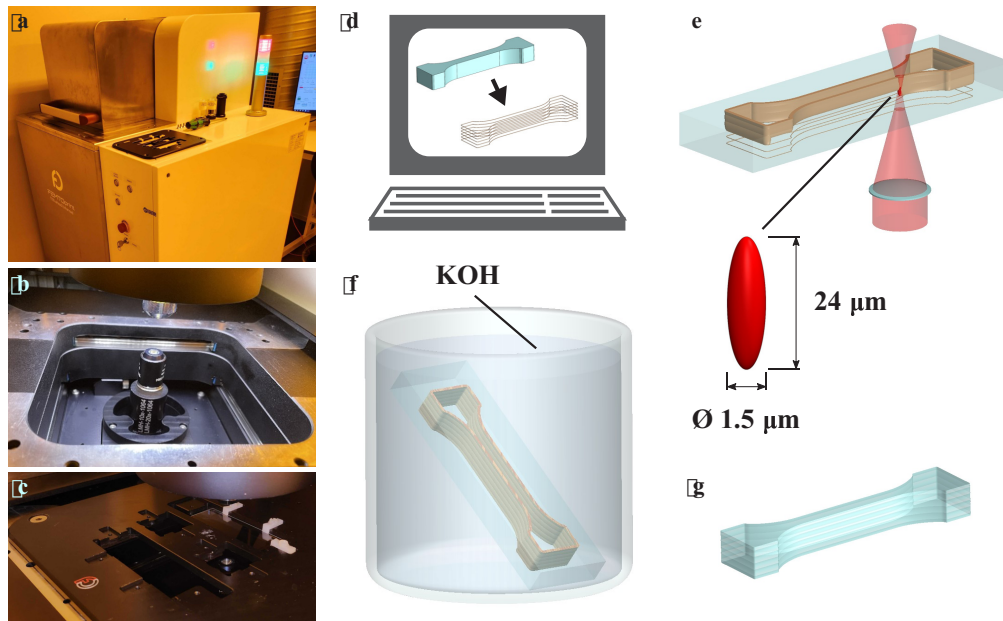


**Fig. 2.** Femtosecond laser-assisted etching. **a** The FEMTOprint device is used to perform the laser exposure step. **b** The laser objective is located at the bottom. The microscope at the top is used to calibrate the position and orient the glass substrate correctly. **c** The glass substrate is attached on a holder placed above the laser objective, itself fixed to a moving stage. **d** The laser path is extracted from the 3D model of the designed part. **e** Laser exposure step: the laser path begins at the top of the substrate and finishes at the surface in front of the laser objective. The laser exposed volume is defined by the laser path and the laser voxel dimension. The dimension is assumed according to the FEMTOprint parameters and not measured. The voxel dimension depends on the focusing conditions and laser parameters. (For representation purposes, the proportions are not accurate) **f** Etching step: the substrate is placed in KOH bath at 85 °C for wet etching. **g** After etching, the finished part is cleaned with pure water.

As depicted in Fig. 2(d), the laser path is defined by extracting the contours of the shape at different heights according to the laser voxel pitch. Depending on the targeted design the laser path will strongly differ. If we want to cut the whole glass the optimal space between two modified planes is 7  $\mu\text{m}$ . So for a 500  $\mu\text{m}$  thick glass plate there are 72 modified planes by femtosecond laser to provide an efficient vertical wet etching. For the planar operation to apply on mechanical structures we have plane one layer but the laser paths are spaced by 3  $\mu\text{m}$  without overlapping on

each other. Next, depending on the type of modifications to be created, the parameters of the laser are adjusted. The glass substrate is then exposed to the focused femtosecond pulse laser, using the FEMTOprint machine following the designed path file. The establishment of the laser path constitutes a crucial process. Presently, the laser path for both the mechanical structures and optical structures is constructed within a unified procedure. Subsequently, the entire plate is etched. However, to safeguard the optical waveguide from being etched, a margin of a few micrometers is kept without laser modification. For a more comprehensive understanding, it is noteworthy that the waveguide and the Bragg grating are constructed at the same level, with the inscription of the waveguide preceding the inscription of the Bragg grating.

The machine includes a focusing microscope objective located under a 3-axis linear moving platform on which the glass substrate is attached. Hence, the femtosecond laser pulses hit the glass substrate from the bottom (Fig. 2(e)). The other microscope objective positioned on top of the substrate is used for visualization purposes on the control software. To shape the material after this irradiation process, the substrate is placed in a temperature-controlled ultrasonic chemical bath for etching (sketch of Fig. 2(f)). To allow a homogeneous and constant temperature of 85 °C, the substrate is placed inside a potassium hydroxide (12 M) recipient in polypropylene. The laser-exposed glass volume is etched much more faster than the non-exposed volume with a ratio of 200:1. Finally, the resulting part is cleaned with pure water and dried at ambient temperature. It allows to get the shaped substrate sketched in Fig. 2(g). The time of creation of a structure can be split into two parts: the inscription with the femtosecond laser and the chemical etching. Both of them can vary according to the shape of the structure. For the current application, the inscription takes 10 hours while the chemical etching lasts 8 hours.

## 2.2. Optical characterization

In terms of characterization, several devices were used to analyse the manufactured structures. First of all, two microscopes (VK-X200 3D laser scanning microscope from Keyence and Axio imager from Zeiss) were used for optical characterization. They allow to observe the roughness and measure the size of the flexible structures. Then, experimental setups were implemented to analyse the spectral quality of the developed optical structures. The reflected amplitude spectra were measured using a broadband optical source and an optical spectrum analyzer (OSA) from Yokogawa (Model AQ6370D). For temperature and axial strain characterizations, we relied on a more accurate interrogator dedicated to fibre Bragg gratings, featuring a wavelength resolution of 1 pm and a repetition rate of 1 Hz. The latter is the Fibresensing FS2200 industrial Braggmeter. Standard telecommunication-grade optical fibres were used to inject light from the source to the manufactured waveguide and collect its signal.

## 2.3. Strain sensing

We want to design a glass flexible structure containing a waveguide and a Bragg grating. This tensile specimen has been specifically conceived to enable a homogeneous strain distribution when subject to load. An experiment has also been conducted to verify the linearity of our Bragg grating sensor. The strain measured with the Bragg grating sensor has been compared to the strain estimated with Hook's law  $\hat{\epsilon}$  in [ $\mu\epsilon$ ]:

$$\hat{\epsilon} = \frac{\sigma}{E_{\text{SiO}_2}} \cdot 10^6 \quad (6)$$

with  $E_{\text{SiO}_2}$ , the elastic modulus of our fused silica glass provided by Siegert Wafer GmbH (72 GPa), and  $\sigma$ , the stress resulting from the applied load and the geometry of the structure. The experiment is designed such that it stays in the fused silica elastic domain (the tensile strength  $\sigma_{\text{adm}}$  for our geometry is estimated above 1 GPa [6]). For a tensile specimen, the stress along its

length is described by :

$$\sigma = \frac{F_{\text{load}}}{S} \quad (7)$$

with  $F_{\text{load}}$ , the applied load, and  $S$ , the cross-section of the specimen. It allows for estimating the strain precisely and homogeneously through the entire plate without considering the BG's location in the specimen. This structure is then analysed in terms of temperature and axial strain gradients. Those results would then be useful to design Bragg grating sensors in flexible structures and define their sensitivities according to their geometry and the position of the Bragg Grating.

The axial strain sensitivity characterization is performed with a voice-coil actuator. The experimental setup and its scheme are presented in Fig. 3. The force applied at the free end of the tensile specimen  $F_{\text{VCA}}$  is commanded by an analogical output of the National Instrument Multifunction I/O device (USB - 6002). A custom current amplifier ( $0.2 \text{ AV}^{-1}$ ) is used to generate a current that drives the voice-coil actuator ( $1.53 \text{ NA}^{-1}$ ) according to the applied voltage. The tensile specimen that is uniform along its length is subject to stress defined by Eq. (7), with  $F_{\text{load}} = F_{\text{VCA}}$ , and  $S$ , its cross section ( $47.5 \times 207 \text{ } \mu\text{m}^2$ ).

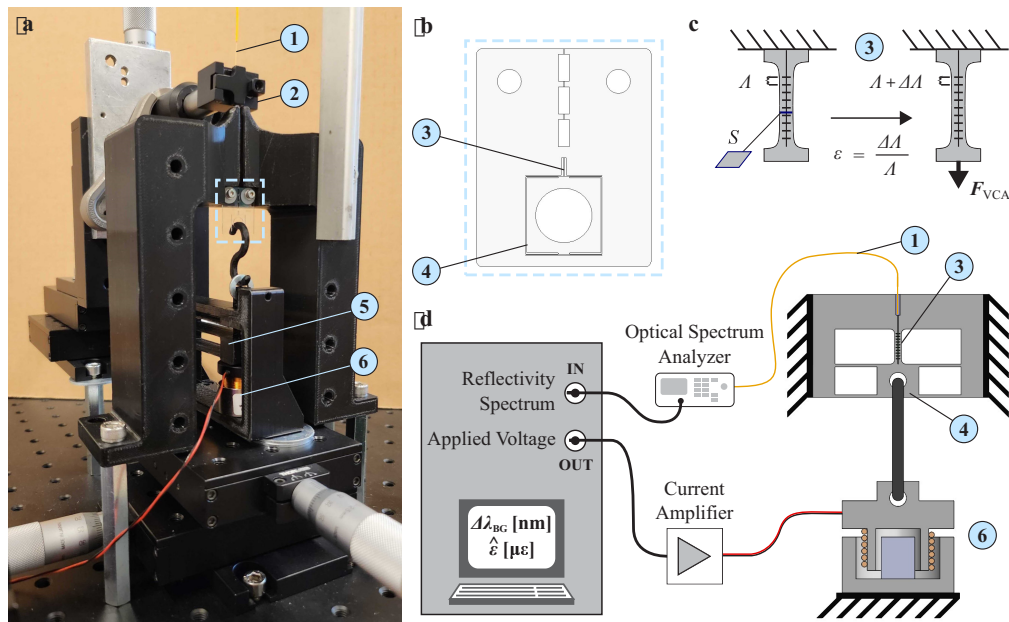


**Fig. 3.** Testbench developed to characterize the axial strain sensitivity of a Bragg Grating sensor inscribed in a fused silica tensile specimen. **a** The tensile specimen (in the blue square) is hanging fixed by two screws. The optical fibre (1) connected to the Bragg interrogator is placed at the top. A fibre clamp (2) is used to position the fibre. **b** The tensile specimen contains a Bragg grating which undergoes a strain  $\epsilon$  when the force  $F_{\text{VCA}}$  is applied at its free end. **c** Experimental scheme: the optical fibre (1) is guided to interface with the tensile specimen (3); the load is applied with a voice-coil actuator (VCA) (6); the moving coil is guided in translation using a monolithic 3D printed flexure mechanism (5); A LabVIEW platform records the reflected spectrum from the interrogator and the applied voltage commanding the VCA; the estimated applied axial strain  $\hat{\epsilon}$  and its resulting Bragg grating wavelength shift  $\Delta\lambda_{\text{BG}}$  are obtained by post-processing with MATLAB.



#### 2.4. Temperature sensing

The setup for temperature characterization is represented in Fig. 4 and allows to record the evolution of the Bragg wavelength of the grating in reflection mode. For temperature calibration, we used a Peltier with a PID (proportional-integral-derivative) temperature controller and external thermo-couple to measure the temperature change at the vicinity of the sample.

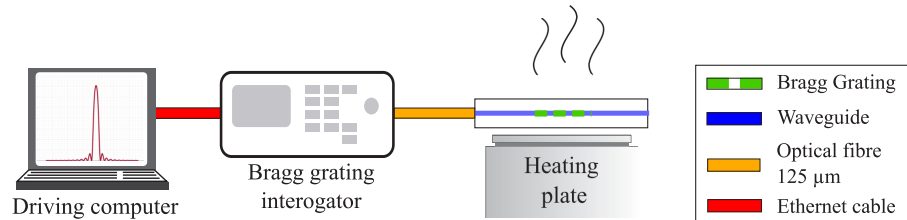


Fig. 4. Characterization setup for the Bragg grating measurements in reflection mode.

### 3. Results

In this section, we summarize the main results obtained with the instrumented glass flexible structures. First of all, Fig. 5 summarizes the main achievements of the manufacturing of Bragg grating-instrumented flexible optical structures using femtosecond pulse laser. The tensile specimen sketched in Fig. 5(a) is produced with the FEMTOprint device. The shaped structure is then placed in a KOH bath for perfect etching of the matter.

To ensure that it is subject to pure axial strain, the Bragg grating is placed along the length of a tensile specimen contained in the processed monolithic structure represented in Fig. 5(a). The apparent circular structure in Fig. 5(b) links the specimen to a linear force actuator. To monitor the deformation, the Bragg grating is inscribed in the femtosecond pulse-induced waveguide. This latter is connected to the measurement device through a single mode optical fibre. To avoid any Fabry-Perot resonance the optical fibre in contact with the glass plate is immersed in refractive index matching gel. The waveguide represented in Fig. 5(c) shows the evolution and the importance of the space between the different laser paths to obtain the waveguide. Fig. 5(d) is made of several laser paths overlapping each other at low energy (130 nJ) until a homogeneous waveguide is created [39]. The length of the waveguide is about 2.75 mm, while the length of the Bragg grating is 1.5 mm. Then, a second order Bragg grating with a pitch of 1.1  $\mu\text{m}$  is inscribed in the core of the optical waveguide with an average energy of 150 nJ. It is schematically represented in Fig. 5(e) and shown with a microscope picture in Fig. 5(f). This Bragg grating is measured in reflection mode, thanks to the experimental setup sketched in Fig. 5(g) and depicted in Fig. 5(h). The reflected amplitude spectrum of the unstrained in-built grating at room temperature is shown in Fig. 5(i). This is the initial measurement for the subsequent axial strain characterization. The full width at half maximum of the main reflection lobe is  $\approx 400$  pm, which is consistent with the actual grating length.

In the following, a fibersensing interrogator was used to record the evolution of the Bragg wavelength shift as a function of temperature and applied strain. Two characterizations setups were implemented. The setup for temperature characterization is represented in Fig. 6 and allows to record the evolution of the Bragg wavelength of the grating in reflection mode. The temperature characterization depicted in Fig. 6 shows the Bragg wavelength shift as a function of a temperature increase between 0 and 90  $^{\circ}\text{C}$  starting from ambient temperature (20  $^{\circ}\text{C}$ ). To show the repeatability of the experiments, six characterizations were conducted on the same sample and then the average value and the corresponding standard deviation were processed for each measurement. A linear regression of the raw data provides a temperature sensitivity of 10.51

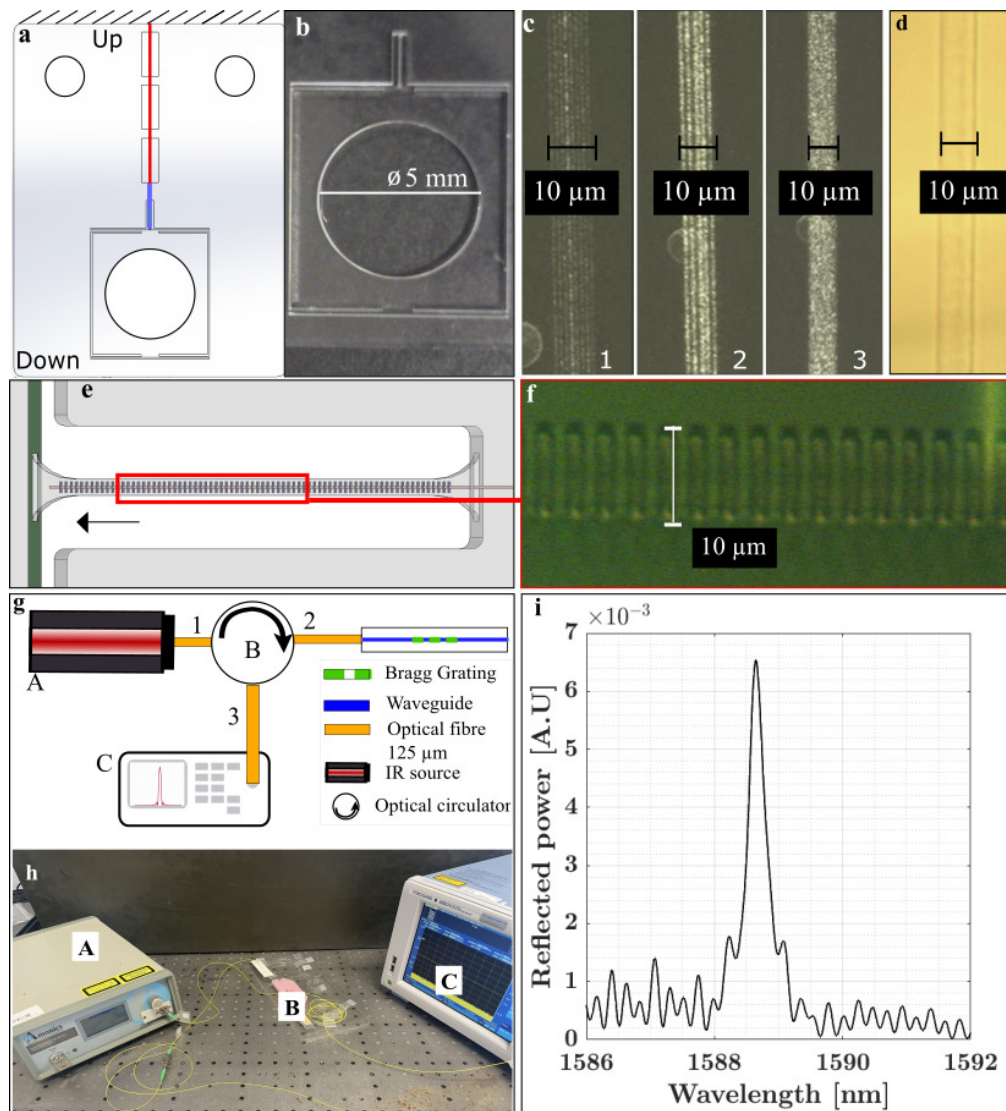


**Fig. 5.** **a** Sketch of the glass flexible structure containing a femtosecond pulse-induced optical waveguide and a Bragg grating within (blue line) and rectangular slots for the easy insertion and coupling of the connecting optical fibre (red line). **b** Picture of the upper part of the structure manufactured by the Femtoprint process and etched in KOH solution. **c** Microscope pictures of different waveguides produced with 3 different spaces between the laser paths; (1) 3  $\mu\text{m}$ , (2) 1.5  $\mu\text{m}$  and (3) 0.5  $\mu\text{m}$ ; (3) is considered to be the most optimal space based on our observations. **d** Microscope picture of the 0.5  $\mu\text{m}$  spaced waveguide taken with an oil-immersion objective. **e** Sketch of the flexible section containing the waveguide and Bragg grating (blue line in **a**). **f** Microscope picture of the plane-by-plane Bragg grating. **g** Scheme of the experimental setup used to characterize the in-built Bragg grating in reflection. **h** Picture of the actual setup. **i** Reflected amplitude spectrum of the Bragg grating measured at rest.

pm/°C, which is consistent with the theoretical and the measurements obtained in silica optical fibres.

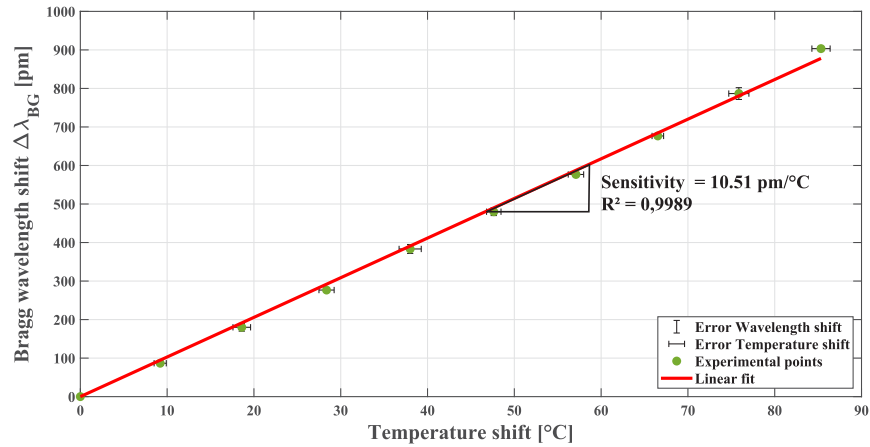


**Fig. 6.** Evolution of the Bragg wavelength as a function of the temperature. For this measurement, the same sample was measured 3 times. The error bars represent the average standard deviation for the same batch.

For the strain calibration, we rely on the experimental setup depicted in Fig. 3. The experimental Bragg grating wavelength shift in response to axial strain is reported in Fig. 7. This Bragg wavelength shift is determined as a difference between the strained and the unstrained specimen. The experimental setup is placed in a confined space to mitigate possible impacts of air fluctuations during the experiment. The linear regression of the raw data yields an axial strain sensitivity of 1.22 pm/μϵ, which is about 10 per cent higher than what is usually obtained in optical fibres but remains in good agreement with the theoretical predictions for the planar substrate.

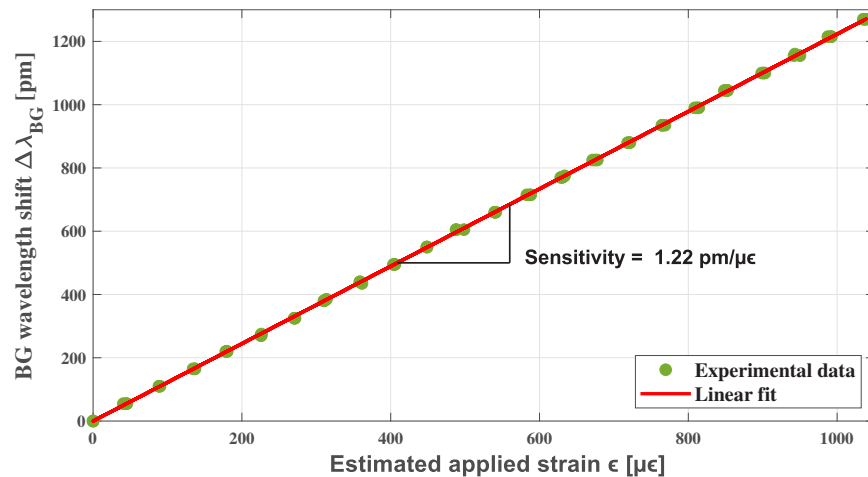


**Fig. 7.** Evolution of the Bragg wavelength as a function of the axial strain application. For this measurement, the same sample was measured 3 times.

#### 4. Discussion

Entirely relying on the same femtosecond pulse laser based-device, we designed and developed an inline instrumented 3D glass structure. Through several optimizations of the writing process, we succeeded in shaping a glass substrate to turn it into a monolithic mechanism. We create an optical waveguide inside with a dedicated cavity to align and optimize the coupling to an optical fibre. A Bragg grating was finally added to the waveguide and characterized to get its response to temperature changes and axial strain. We have selected a specific design for the flexible structure in order to ensure the coherence between the applied load and the resulting axial strain in the tensile specimen. As shown in Fig. 5(a), its free end is guided in translation by a monolithic compliant mechanism (that is described in Fig. 3). Although being a non-linear mechanism, it is frequently used for small displacements. Thus, in a quasi-linear regime, as in Athanasiou's work [33], also used to load a tensile specimen, it is particularly interesting for its design simplicity and limited required volume. The force-displacement characteristic of this type of mechanism has been computed by S. Henein [40]. It can be approximated for a quasi-linear regime as:

$$F_{\text{guidance}} \approx \frac{4E_{\text{SiO}_2}bh^3}{l^3}f \quad (8)$$

with respectively the width  $b$ , 500  $\mu\text{m}$ , the thickness  $h$ , 50  $\mu\text{m}$ , and the length  $l$ , 3 mm, of the guidance blades and  $f$ , their deflection that corresponds to the elongation of the tensile specimen  $\Delta L = \hat{\epsilon}L$ , with  $L$ , the length of the tensile specimen (1.5 mm, corresponding to the grating length). To quantify the influence of the guidance on the accuracy of our sensor, let us compute its resulting wavelength shift variation for a large measurement. We then take  $\Delta\lambda_{\text{BG}} = 1220$  pm. Considering the obtained sensitivity, it corresponds to a strain of 1000  $\mu\epsilon$ . Then, using Eq. (8), the restoring force of the guidance is of the order of 1 mN. By applying Eqs. (6) and (7), it corresponds to a resulting strain variation of about 1.5  $\mu\epsilon$ , yielding a wavelength difference of  $\approx 1.8$  pm. It is close to the wavelength resolution of the measurement device and the guidance contribution can therefore be neglected due to its small value.

The obtained axial strain and temperature sensitivities of our sensor confirm that it is compliant with the well-known FBG theory. The small difference between the experimental results and the theoretical model can be explained by the tensile specimen cross-section measurement error ( $\pm 2.5$   $\mu\text{m}$  for thickness and  $\pm 5$   $\mu\text{m}$  for width) and by the elastic modulus given by the glass substrate manufacturer. These dimensions are used to estimate the applied strain according to the applied force. It can also be explained by the tolerance of the Poisson's ratio and the elasto-optic coefficients of the fused silica glass substrate that were used to define the theoretical sensitivity.

It is also worth mentioning that the interface between the optical fibre and the written waveguide was a critical design step to limit the intensity loss. The thin 0.5 mm glass substrate made it difficult to interface our structure with a standard ferrule for telecommunication-grade optical fibres. Therefore, a custom interface has been designed and optimized by an iterative method to align the fibre with the waveguide and ensure an easy insertion. The three squared holes are placed such as the fibre is guided along a sufficient length and the etching time required to generate the cavities remains limited (8 hours). The guiding cavities are 126  $\mu\text{m}$  large and 0.5 mm long and the squared holes are 1 mm large. They also allow to facilitate the removal of an eventually broken fibre.

#### 5. Conclusion

In this paper, we have instrumented a glass flexible structure entirely using focused femtosecond laser pulse delivered by the Femtoprint machine. A planar substrate has first been shaped to produce an innovative tensile specimen allowing a uniform distribution of the strain along its flexible part when it is subject to load. An optical waveguide, a Bragg grating and an optical

fibre holder have also been designed and manufactured using the Femtoprint, with appropriate pulse energies and translation speed in each case. High performances have been obtained and the reflected amplitude spectrum of the in-built grating can be easily measured with a standard fibre Bragg grating interrogator (or data acquisition system). The engineered sensing platform has been characterized for axial strain and temperature sensing, confirming that the obtained sensitivities (respectively 1.22 pm/ $\mu\epsilon$  and 10.51 pm/ $^{\circ}\text{C}$ ) are conformed to the expectations. This sensing platform is an innovative structure due to its level of integration and the fact that we are able to create the waveguide and the mechanical structure in the same process. This first experimental demonstration of precise temperature and axial strain monitoring of glass mechanism at microscales is a starting point for many different possibilities of application. Upon small modifications in design, such structures could be used either in the field of deformation monitoring or even biosensing.

**Funding.** Fonds De La Recherche Scientifique - FNRS (T.0049.20).

**Acknowledgments.** The authors gratefully acknowledge the "Fonds de la Recherche Scientifique", Research project grant INFuSE (grant agreement number FNRS PDR T.0049.20), for funding this research.

**Disclosures.** The authors declare that there are no conflicts of interest related to this article.

**Data availability.** The data that support the findings of this study are available from the corresponding author upon reasonable request.

## References

1. M. Malinauskas, A. Žukauskas, S. Hasegawa, Y. Hayasaki, V. Mizeikis, R. Buividas, and S. Juodkazis, "Ultrafast laser processing of materials: from science to industry," *Light: Sci. Appl.* **5**(8), e16133 (2016).
2. X. Wang, H. Yu, P. Li, Y. Zhang, Y. Wen, Y. Qiu, Z. Liu, Y. Li, and L. Liu, "Femtosecond laser-based processing methods and their applications in optical device manufacturing: A review," *Opt. Laser Technol.* **135**, 106687 (2021).
3. R. R. Gattass and E. Mazur, "Femtosecond laser micromachining in transparent materials," *Nat. Photonics* **2**(4), 219–225 (2008).
4. Y. Bellouard, A. Said, M. Dugan, and P. Bado, "Fabrication of high-aspect ratio, micro-fluidic channels and tunnels using femtosecond laser pulses and chemical etching," *Opt. Express* **12**(10), 2120–2129 (2004).
5. M. Beresna, M. Gecevičius, and P. G. Kazansky, "Ultrafast laser direct writing and nanostructuring in transparent materials," *Adv. Opt. Photonics* **6**(3), 293–339 (2014).
6. Y. Bellouard, "On the bending strength of fused silica flexures fabricated by ultrafast lasers," *Opt. Mater. Express* **1**(5), 816–831 (2011).
7. C. Hnatovsky, R. Taylor, P. Rajeev, E. Simova, V. Bhardwaj, D. Rayner, and P. Corkum, "Pulse duration dependence of femtosecond-laser-fabricated nanogratings in fused silica," *Appl. Phys. Lett.* **87**(1), 014104 (2005).
8. A.-C. Tien, S. Backus, H. Kapteyn, M. Murnane, and G. Mourou, "Short-pulse laser damage in transparent materials as a function of pulse duration," *Phys. Rev. Lett.* **82**(19), 3883–3886 (1999).
9. A. P. Joglekar, H.-h. Liu, G. Spooner, E. Meyhöfer, G. Mourou, and A. Hunt, "A study of the deterministic character of optical damage by femtosecond laser pulses and applications to nanomachining," *Appl. Phys. B* **77**(1), 25–30 (2003).
10. P. G. Kazansky, W. Yang, E. Bricchi, J. Bovatsek, A. Arai, Y. Shimotsuma, K. Miura, and K. Hirao, "Quill writing with ultrashort light pulses in transparent materials," *Appl. Phys. Lett.* **90**(15), 151120 (2007).
11. K. Chah, D. Kinet, M. Wuilpart, P. Mégret, and C. Caucheteur, "Femtosecond-laser-induced highly birefringent bragg gratings in standard optical fiber," *Opt. Lett.* **38**(4), 594–596 (2013).
12. K. Zhou, M. Dubov, C. Mou, L. Zhang, V. K. Mezentsev, and I. Bennion, "Line-by-line fiber bragg grating made by femtosecond laser," *IEEE Photonics Technol. Lett.* **22**(16), 1190–1192 (2010).
13. M. Will, S. Nolte, B. N. Chichkov, and A. Tünnermann, "Optical properties of waveguides fabricated in fused silica by femtosecond laser pulses," *Appl. Opt.* **41**(21), 4360–4364 (2002).
14. J. Canning, M. Lancry, K. Cook, A. Weickman, F. Brisset, and B. Poumellec, "Anatomy of a femtosecond laser processed silica waveguide," *Opt. Mater. Express* **1**(5), 998–1008 (2011).
15. X. Liu, D. Du, and G. Mourou, "Laser ablation and micromachining with ultrashort laser pulses," *IEEE J. Quantum Electron.* **33**(10), 1706–1716 (1997).
16. R. S. Taylor, C. Hnatovsky, E. Simova, D. M. Rayner, M. Mehandale, V. Bhardwaj, and P. Corkum, "Ultra-high resolution index of refraction profiles of femtosecond laser modified silica structures," *Opt. Express* **11**(7), 775–781 (2003).
17. S. Kiyama, S. Matsuo, S. Hashimoto, and Y. Morihira, "Examination of etching agent and etching mechanism on femtosecond laser microfabrication of channels inside vitreous silica substrates," *J. Phys. Chem. C* **113**(27), 11560–11566 (2009).

18. A. Marcinkevičius, S. Juodkazis, M. Watanabe, M. Miwa, S. Matsuo, H. Misawa, and J. Nishii, "Femtosecond laser-assisted three-dimensional microfabrication in silica," *Opt. Lett.* **26**(5), 277–279 (2001).
19. E. Casamenti, S. Pollonghini, and Y. Bellouard, "Few pulses femtosecond laser exposure for high efficiency 3d glass micromachining," *Opt. Express* **29**(22), 35054–35066 (2021).
20. S. Ugale and V. Mishra, "Fiber bragg grating modeling, characterization and optimization with different index profiles," *International Journal of Engineering Science and Technology* **2**, 4463–4468 (2010).
21. A. Othonos, K. Kalli, D. Pureur, and A. Mugnier, "Fibre bragg gratings," in *Wavelength Filters in Fibre Optics*, (Springer, 2006), 189–269.
22. A. Yariv and P. Yeh, *Optical waves in crystals*, vol. 5 (Wiley New York, 1984).
23. R. Kashyap, *Fiber Bragg gratings* (Academic press, 2009).
24. A. Martínez, I. Y. Khrushchev, and I. Bennion, "Direct inscription of Bragg gratings in coated fibers by an infrared femtosecond laser," *Opt. Lett.* **31**(11), 1603–1605 (2006).
25. A. Theodosiou, A. Lacraz, A. Stassis, C. Koutsides, M. Komodromos, and K. Kalli, "Plane-by-plane femtosecond laser inscription method for single-peak bragg gratings in multimode cytop polymer optical fiber," *J. Lightwave Technol.* **35**(24), 5404–5410 (2017).
26. G. Laffont, R. Cotillard, N. Roussel, R. Desmarchelier, and S. Rougeault, "Temperature resistant fiber bragg gratings for on-line and structural health monitoring of the next-generation of nuclear reactors," *Sensors* **18**(6), 1791 (2018).
27. S. J. Mihailov, D. Grobnc, C. Hnatovsky, R. B. Walker, P. Lu, D. Coulas, and H. Ding, "Extreme environment sensing using femtosecond laser-inscribed fiber bragg gratings," *Sensors* **17**(12), 2909 (2017).
28. I.-B. Sohn, H.-K. Choi, Y.-C. Noh, J. Kim, and M. S. Ahsan, "Laser assisted fabrication of micro-lens array and characterization of their beam shaping property," *Appl. Surf. Sci.* **479**, 375–385 (2019).
29. M. Sakakura, Y. Lei, L. Wang, Y.-H. Yu, and P. G. Kazansky, "Ultralow-loss geometric phase and polarization shaping by ultrafast laser writing in silica glass," *Light: Sci. Appl.* **9**(1), 15 (2020).
30. D. Tan, X. Sun, and J. Qiu, "Femtosecond laser writing low-loss waveguides in silica glass: highly symmetrical mode field and mechanism of refractive index change," *Opt. Mater. Express* **11**(3), 848–857 (2021).
31. M. Thiel, G. Flachenecker, and W. Schade, "Femtosecond laser writing of bragg grating waveguide bundles in bulk glass," *Opt. Lett.* **40**(7), 1266–1269 (2015).
32. E. Casamenti, T. Yang, P. Vlugter, and Y. Bellouard, "Vibration monitoring based on optical sensing of mechanical nonlinearities in glass suspended waveguides," *Opt. Express* **29**(7), 10853–10862 (2021).
33. C.-E. Athanasiou and Y. Bellouard, "A monolithic micro-tensile tester for investigating silicon dioxide polymorph micromechanics, fabricated and operated using a femtosecond laser," *Micromachines* **6**(9), 1365–1386 (2015).
34. R. N. Widmer, D. Bischof, J. Jurczyk, M. Michler, J. Schwiedrzik, and J. Michler, "Smooth or not: Robust fused silica micro-components by femtosecond-laser-assisted etching," *Mater. Des.* **204**, 109670 (2021).
35. C. Le Losq, M. R. Cicconi, G. N. Greaves, and D. R. Neuville, "Silicate glasses," in *Springer handbook of glass*, (Springer, 2019), 441–503.
36. Y. Bellouard, A. Champion, B. Lenssen, M. Matteucci, A. Schaap, M. Beresna, C. Corbari, M. Gecevicius, P. Kazansky, and O. Chappuis, "The femtoprint project," *J. Laser Micro/Nanoeng.* **7**(1), 1–10 (2012).
37. R. Ben Hassen, "Design and development of a 3 dof force sensor using fiber bragg gratings in endoscopic applications," Ph.D. thesis, Université libre de Bruxelles, (2023).
38. S. Rajesh and Y. Bellouard, "Towards fast femtosecond laser micromachining of fused silica: The effect of deposited energy," *Opt. Express* **18**(20), 21490–21497 (2010).
39. G. D. Marshall, M. Ams, and M. J. Withford, "Direct laser written waveguide-bragg gratings in bulk fused silica," *Opt. Lett.* **31**(18), 2690–2691 (2006).
40. F. Cosandier, S. Henein, M. Richard, and L. Rubbert, *The art of flexure mechanism design* (Epl Press, 2017).